Electronic Supplementary Material (ESI) for Physical Chemistry Chemical Physics.


# Revival of collective water structure and dynamics in reverse micelles brought about by protein encapsulation

## Supplementary Information

Philipp Honegger and Othmar Steinhauser

## Geometry

We address the conformational stability of UBQ as monitored by the radius of gyration $r_{\mathrm{gyr}}$ representing a measure of protein compactness. Its temporal evolution is shown in the top panel of the figure below. We observe a contraction of $\approx 0.5$ Å in the initial time period of 100 ns for all $\lambda$-scalings. Afterwards, $r_{\mathrm{gyr}}$ remains stable for the complete simulation run. For this reason, all trajectory analyses in the main article were started at the 100 ns mark. This result is important as it shows that fluctuations of the UBQ dipole are mainly rotational in character and not brought about by conformational changes. The tendency for proteins to favor compact conformations in crowded or encapsulated environment has been pointed out previously[1] and may result from stabilization by decreased hydration of encapsulated proteins observed both empirically and in simulation[2–5].

In order to properly address the electric anisotropy shown by the dielectric properties, we shortly analyze the spatial anisotropy of the RM. This can be done by considering the radial distance $R(\theta, \phi, t)$ of a vector originating from the RM center of mass and joining a surface element orientated in the direction descibed by the polar angles $\theta$ and $\phi$. The resulting bundle of vectors is exemplified in the graphic at the right of the figure below. The temporal fluctuation of the distribution of $R(\theta, \phi, t)$ can be expanded as a linear combination of spherical

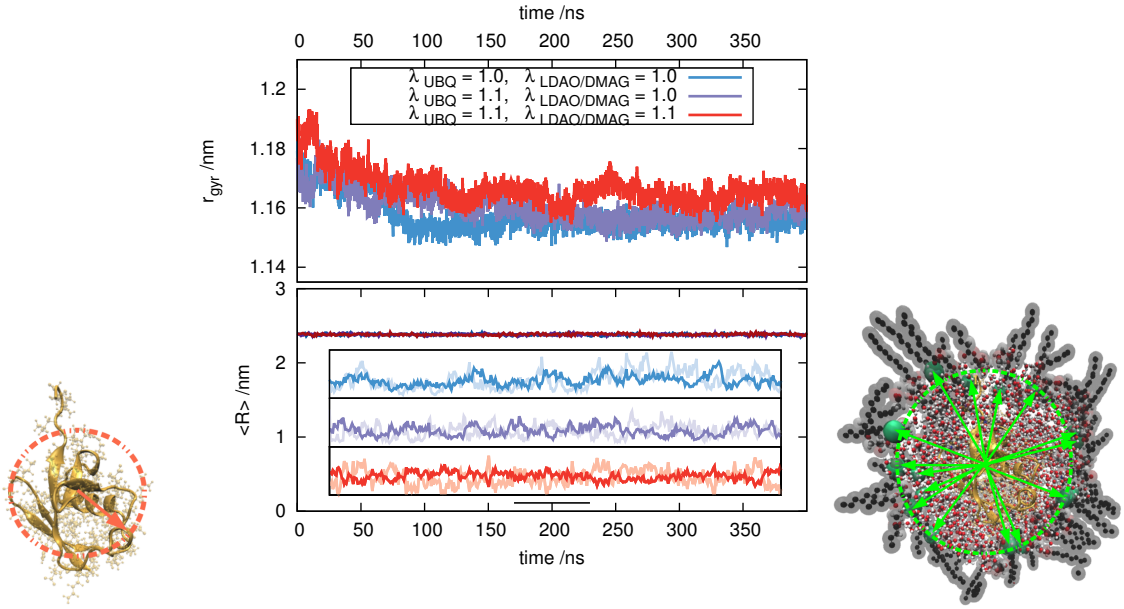


Top panel: Radius of gyration $r_{\mathrm{gyr}}$ of the UBQ molecule as a function of time. The three levels of $\lambda$-scaling are shown in blue (unscaled), purple (half-scaled) and red (fully scaled).
Bottom panel: Temporal evolution of the RM radius $r_{RM}$ calculated from $C_0^0$ of the vectors connecting the RM center of mass with the LDAO nitrogens as representatives of the RM surface elements.
Insets in bottom panel: $C_m^{l*}C_m^l$ terms with l = 1. These parameters show asphericity. The pale lines and the bright lines represent the terms $C_0^{1*}C_0^1$ and $C_1^{1*}C_1^1 = C_{-1}^{1*}C_{-1}^1$ respectively. The three levels of scaling are disentangled in the three insets.

harmonics $Y_m^l(\theta, \phi)$:

$$R(t, \theta, \phi) = \sum_{l=0}^{\infty} \sum_{m=-l}^{m=+l} C_m^l(t) Y_m^l(\theta, \phi) \tag{1}$$

In this harmonic analysis, the product $C_m^{l*} C_m^l$ is the probability for the population of a certain angular space. This type of analysis was first used for RMs by Brown and Clarke[6] who developed this product as a time series and presented the sphericity anisotropy decay. $C_0^0 C_0^0$ stands for a spherical RM with $C_0^0$ given by

$$\frac{C_0^0}{\sqrt{4\pi}} = \frac{1}{4\pi} \int d\Omega R(\Omega, t) = \langle R(t) \rangle \tag{2}$$

yielding the average radius of the RM at time $t$. The RM radius $r_{RM} = \langle R \rangle$ is shown in the bottom panel of above figure. The higher coefficients $C_m^{l*} C_m^l$ with $l > 0$ are a measure of anisotropy. Two of them, $C_1^{1*} C_1^1 = C_{-1}^{1*} C_{-1}^1$ as well as $C_0^{1*} C_0^1$ are shown in the bottom panel of above figure. While both $\langle R \rangle$ and the anisotropy terms fluctuate, this fluctuation is antagonistic and never strays far from the perfect spherical shape. Hence, no systematic trends indicative of an inherent asphericity can be observed. It is remarkable that insertion of a protein into an RM preserves sphericity. This effect is probably brought about by the tendency of water surface minimization. AOT RMs, on the other hand, are known to be aspherical[3,7], particularly for small water loadings $w_0$ [8] and if they do not contain a solute[9], possibly due to distortions caused by the strong ionic interactions in a limited space.

# Single-particle dynamics of water

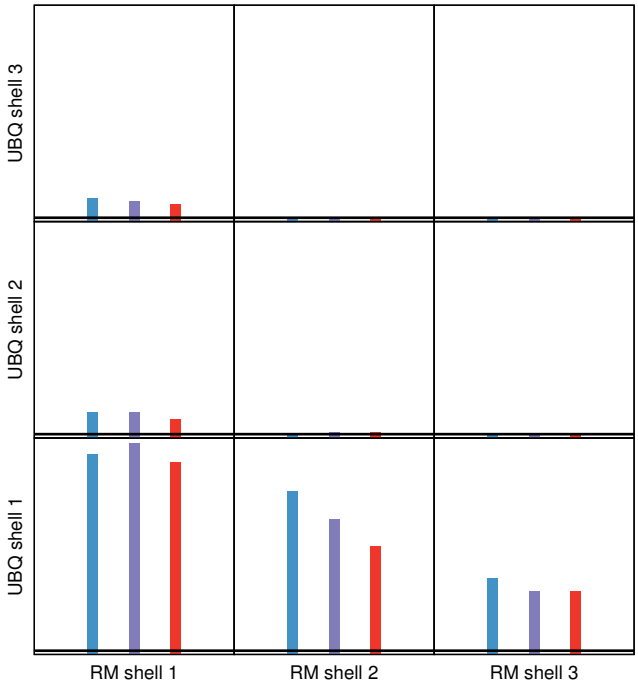


Shell-specific single-particle reorientational relaxation times. For reasons of statistical stability, only the innermost, strongest occupied $3 \times 3$ submatrix shown in Fig. 7 in the main article was analyzed. The vertical bars show the respective $\tau_{sp}$ for the unscaled (blue), half-scaled (purple) and the fully scaled (red) systems with respect to the bulk water $\tau_{sp}$ (black line at the bottom of each panel). Each row stands for a certain Delauny distance with regards to the protein surface and each column refers to a Delauny distance from the surfactant wall.
Table below: Numeric relaxation times in picoseconds sorted by shell as integral over the single-particle TCF.

| | | $\tau_{sp}^{unscaled}$ | $\tau_{sp}^{half\text{-}scaled}$ | $\tau_{sp}^{fully\ scaled}$ |
|---|---|---|---|---|
| **RM-shell1** | **UBQ-shell1** | 250.0 | 263.0 | 240.0 |
| | **UBQ-shell2** | 31.9 | 31.9 | 22.8 |
| | **UBQ-shell3** | 29.0 | 25.1 | 21.3 |
| **RM-shell2** | **UBQ-shell1** | 204.2 | 169.3 | 135.4 |
| | **UBQ-shell2** | 5.7 | 6.3 | 6.6 |
| | **UBQ-shell3** | 5.4 | 5.8 | 5.0 |
| **RM-shell3** | **UBQ-shell1** | 95.2 | 78.5 | 78.5 |
| | **UBQ-shell2** | 5.5 | 5.7 | 6.1 |
| | **UBQ-shell3** | 4.8 | 5.1 | 5.9 |

# $\lambda$-scaling

This section describes the $\lambda$-scaling of the water-interface interactions performed for this study. Petrov and Zagrovic have pointed out flawed protein dynamics such as exaggerated aggregation behaviour brought about by current force fields[10]. Best, Mittal *et al.*[11] showed that rescaling the potential well depth $\epsilon_{ij}$ of the Lennard-Jones potential

$$U_{ij}^{\mathrm{LJ}}(r_{ij}) = 4\epsilon_{ij}\{(\frac{\sigma_{ij}}{r_{ij}})^{12} - (\frac{\sigma_{ij}}{r_{ij}})^{6}\} \tag{3}$$

comes with remarkable improvements in solvation energy and protein-protein interaction behaviour. CHARMM force fields do not store pair-wise Lennard-Jones distance and interaction parameters $\sigma_{ij}$ and $\epsilon_{ij}$, but atom parameters $\sigma_i$ and $\epsilon_i$, which are combined for each pair by the Lorenz-Berthelot relations

$$\sigma_{ij} = \frac{1}{2}(\sigma_i + \sigma_j) \tag{4}$$

$$\epsilon_{ij} = (\epsilon_i \epsilon_j)^{\frac{1}{2}} \tag{5}$$

In Bests and Mittals approach, $\epsilon$ and thus the entire shape of the dispersion interaction is then simply re-scaled by

$$\epsilon_{ij}^{\text{scaled}} = \lambda\epsilon_{ij} \tag{6}$$

with $\lambda = 1.1$ being sufficient to yield more realistic protein behaviour[11,12]. The thus adjusted interaction parameters were imposed on the force field after loading all parameters using the NBFIX key word. The tables below list the NBFIX parameters for the system with only the protein-water interactions adjusted and the NBFIX commands for the system with both protein-water and surfactant-water interaction being adjusted, respectively. The first column contains the SPC/E water oxygen only, since the hydrogen does not exert dispersion interaction in this model. The second column lists the CHARMM36[13–16] force field atom types representing protein- and surfactant atoms.

NBFIX commands for the half-scaled system ($\lambda_{\mathrm{H_2O,\,UBQ}} = 1.1, \lambda_{\mathrm{H_2O,\,LDAO/DMAG}} = 1.0$)

| **atom type 1** | **atom type 2** | $\epsilon$ | $\sigma$ |
|---|---|---|---|
| OT | C | -0.142283 | 3.777 |
| OT | CA | -0.113503 | 3.7694 |
| OT | CC | -0.113503 | 3.777 |
| OT | CD | -0.113503 | 3.777 |
| OT | CE1 | -0.11187 | 3.867 |
| OT | CE2 | -0.108529 | 3.857 |
| OT | CP1 | -0.06067 | 4.052 |
| OT | CP2 | -0.100609 | 3.952 |
| OT | CP3 | -0.100609 | 3.952 |
| OT | CPH1 | -0.095927 | 3.577 |
| OT | CPH2 | -0.095927 | 3.577 |
| OT | CS | -0.142283 | 3.977 |
| OT | CPT | -0.134982 | 3.637 |
| OT | CY | -0.115909 | 3.767 |
| OT | CAI | -0.115909 | 3.767 |
| OT | CT | -0.06067 | 4.052 |
| OT | CT1 | -0.076742 | 3.777 |
| OT | CT2 | -0.10152 | 3.787 |
| OT | CT2A | -0.10152 | 3.787 |
| OT | CT3 | -0.119813 | 3.817 |
| OT | H | -0.09201 | 2.0015 |
| OT | HA | -0.063631 | 3.097 |
| OT | HB1 | -0.063631 | 3.097 |
| OT | HB2 | -0.071785 | 3.117 |
| OT | HE1 | -0.075533 | 3.027 |

| | | | |
|---|---|---|---|
| OT | HE2 | -0.069174 | 3.037 |
| OT | HB | -0.063631 | 3.097 |
| OT | HC | -0.09201 | 2.0015 |
| OT | HP | -0.074305 | 3.1352 |
| OT | HR1 | -0.09201 | 2.677 |
| OT | HR2 | -0.09201 | 2.477 |
| OT | HR3 | -0.037888 | 3.245 |
| OT | HS | -0.135662 | 2.227 |
| OT | HA1 | -0.091005 | 3.117 |
| OT | HA2 | -0.079104 | 3.117 |
| OT | HA3 | -0.06646 | 3.117 |
| OT | N | -0.191855 | 3.627 |
| OT | NC2 | -0.191855 | 3.627 |
| OT | NH1 | -0.191855 | 3.627 |
| OT | NH2 | -0.191855 | 3.627 |
| OT | NH3 | -0.191855 | 3.627 |
| OT | NP | -0.191855 | 3.627 |
| OT | NR1 | -0.191855 | 3.627 |
| OT | NR2 | -0.191855 | 3.627 |
| OT | NR3 | -0.191855 | 3.627 |
| OT | NY | -0.191855 | 3.627 |
| OT | O | -0.14861 | 3.477 |
| OT | OB | -0.14861 | 3.477 |
| OT | OC | -0.14861 | 3.477 |
| OT | OH1 | -0.16731 | 3.547 |
| OT | OS | -0.16731 | 3.547 |
| OT | S | -0.287782 | 3.777 |
| OT | SM | -0.264453 | 3.752 |
| OT | SS | -0.294108 | 3.97 |

NBFIX commands for the fully scaled system ($\lambda_{\mathrm{H_2O,\,UBQ}} = 1.1, \lambda_{\mathrm{H_2O,\,LDAO/DMAG}} = 1.1$)

| **atom type 1** | **atom type 2** | $\epsilon$ | $\sigma$ |
|---|---|---|---|
| OT | C | -0.142283 | 3.777 |
| OT | CA | -0.113503 | 3.7694 |
| OT | CC | -0.113503 | 3.777 |
| OT | CD | -0.113503 | 3.777 |
| OT | CE1 | -0.11187 | 3.867 |
| OT | CE2 | -0.108529 | 3.857 |
| OT | CP1 | -0.06067 | 4.052 |
| OT | CP2 | -0.100609 | 3.952 |
| OT | CP3 | -0.100609 | 3.952 |
| OT | CPH1 | -0.095927 | 3.577 |
| OT | CPH2 | -0.095927 | 3.577 |
| OT | CS | -0.142283 | 3.977 |
| OT | CPT | -0.134982 | 3.637 |
| OT | CY | -0.115909 | 3.767 |
| OT | CAI | -0.115909 | 3.767 |
| OT | CT | -0.06067 | 4.052 |
| OT | CT1 | -0.076742 | 3.777 |
| OT | CT2 | -0.10152 | 3.787 |
| OT | CT2A | -0.10152 | 3.787 |
| OT | CT3 | -0.119813 | 3.817 |
| OT | H | -0.09201 | 2.0015 |
| OT | HA | -0.063631 | 3.097 |
| OT | HB1 | -0.063631 | 3.097 |
| OT | HB2 | -0.071785 | 3.117 |
| OT | HE1 | -0.075533 | 3.027 |

| | | | |
|---|---|---|---|
| OT | HE2 | -0.069174 | 3.037 |
| OT | HB | -0.063631 | 3.097 |
| OT | HC | -0.09201 | 2.0015 |
| OT | HP | -0.074305 | 3.1352 |
| OT | HR1 | -0.09201 | 2.677 |
| OT | HR2 | -0.09201 | 2.477 |
| OT | HR3 | -0.037888 | 3.245 |
| OT | HS | -0.135662 | 2.227 |
| OT | HA1 | -0.091005 | 3.117 |
| OT | HA2 | -0.079104 | 3.117 |
| OT | HA3 | -0.06646 | 3.117 |
| OT | N | -0.191855 | 3.627 |
| OT | NC2 | -0.191855 | 3.627 |
| OT | NH1 | -0.191855 | 3.627 |
| OT | NH2 | -0.191855 | 3.627 |
| OT | NH3 | -0.191855 | 3.627 |
| OT | NP | -0.191855 | 3.627 |
| OT | NR1 | -0.191855 | 3.627 |
| OT | NR2 | -0.191855 | 3.627 |
| OT | NR3 | -0.191855 | 3.627 |
| OT | NY | -0.191855 | 3.627 |
| OT | O | -0.14861 | 3.477 |
| OT | OB | -0.14861 | 3.477 |
| OT | OC | -0.14861 | 3.477 |
| OT | OH1 | -0.16731 | 3.547 |
| OT | OS | -0.16731 | 3.547 |
| OT | S | -0.287782 | 3.777 |
| OT | SM | -0.264453 | 3.752 |
| OT | SS | -0.294108 | 3.97 |
| | | | |
| OT | CG2O2 | -0.134298 | 3.477 |
| OT | CG311 | -0.076742 | 3.777 |
| OT | CG321 | -0.10152 | 3.787 |
| OT | CG334 | -0.119043 | 3.992 |
| OT | CH2 | -0.134374 | 4.0612 |
| OT | CH3 | -0.19531 | 3.8805 |
| OT | HGA1 | -0.091005 | 3.117 |
| OT | HGA2 | -0.080259 | 3.117 |
| OT | HGP1 | -0.09201 | 2.0015 |
| OT | HGP5 | -0.09201 | 2.477 |
| OT | NG3P0 | -0.191855 | 3.627 |
| OT | OG2D1 | -0.14861 | 3.477 |
| OT | OG302 | -0.135662 | 3.427 |
| OT | OG311 | -0.188027 | 3.542 |
| OT | OG312 | -0.14861 | 3.527 |

# References


[1] H.-X. Zhou, *Archives of Biochemistry and Biophysics*, 2008, **469**, 76–82.

[2] S. Mukherjee, P. Chowdhury and F. Gai, *J. Phys. Chem. B*, 2006, **110**, 11615–11619.

[3] A. V. Martinez, S. C. DeSensi, L. Dominguez, E. Rivera and J. E. Straub, *J. Chem. Phys.*, 2011, **134**, 055107.

[4] J. Tian and A. E. Garcia, *Biophys. J.*, 2009, **96**, L57–L59.

[5] S. Abel, M. Waks, W. Urbach and M. Marchi, *J. Am. Chem. Soc.*, 2006, **128**, 382–383.

[6] D. Brown and J. H. R. Clarke, *J. Phys. Chem.*, 1988, **92**, 2881–2888.

[7] S. Abel, F. Sterpone, S. Bandyopadhyay and M. Marchi, *J. Phys. Chem. B*, 2004, **108**, 19458–19466.

[8] V. R. Vasquez, B. C. Williams and O. A. Graeve, *J. Phys. Chem. B*, 2011, **115**, 2979–2987.

[9] A. V. Martinez, E. Malolepsza, L. Dominguez, Q. Lu and J. E. Straub, *J. Phys. Chem. B*, 2014, **119**, 9084–9090.

[10] D. Petrov and B. Zagrovic, *PLOS Computational Biology*, 2014, **10**, e1003638.

[11] R. B. Best, W. Zheng and J. Mittal, *J. Chem. Theory Comput.*, 2014, **10**, 5113–5124.

[12] P. Honegger, M. Schmollngruber and O. Steinhauser, *Phys. Chem. Chem. Phys.*, 2018, **20**, 19581–19594.

[13] D. Beglov and B. Roux, *J. Chem. Phys.*, 1994, **100**, 9050.

[14] A. D. M. Jr., D. Bashford, M. Bellott, R. L. D. Jr., J. D. Evanseck, M. J. Field, S. Fischer, J. Gao, H. Guo, S. Ha, D. Joseph-McCarthy, L. Kuchnir, K. Kuczera, F. T. K. Lau, C. Mattos, S. Michnick, T. Ngo, D. T. Nguyen, B. Prodhom, W. E. Reiher, B. Roux, M. Schienkrich, J. C. Smith, R. Stote, J. Straub, M. Watanabe, J. Wlorklewicz-Kuczera, D. Yin and M. Karplus, *J. Phys. Chem. B*, 1998, **102(18)**, 3586–3616.

[15] A. D. M. Jr., M. Feig and C. L. B. III, *J. Am. Chem. Soc.*, 2004, **126**, 698–699.

[16] R. B. Best, X. Zhu, J. Shim, P. E. Lopes, J. Mittal, M. Feig and A. D. M. Jr., *J. Chem. Theory Comput.*, 2012, **8(9)**, 3257–3273.